

Photocatalytic degradation of organic pollutants in wastewater using different nanomaterials immobilized on polymeric beads

R.A. Elkholy^{a,*}, E.M. Khalil^b, A.B. Farag^b, M.M. Abo El-Fadl^a, A.M. El-Aassar^a

^aHydrogeochemistry Department, Desert Research Center, Cairo, Egypt, Tel./Fax: +202 26389069, emails: rasha_ali321@yahoo.com/rasha_ali@erdc.gov.eg (R.A. Elkholy)

^bChemistry Department, Faculty of Science, Helwan University, Cairo, Egypt

Received 6 December 2019; Accepted 12 February 2020

ABSTRACT

The present study is concerned with the photocatalytic degradation process to eliminate the organic pollutants. Sodium alginate (SA) was used as a polymeric substrate and prepared as beads form to increase the surface area and enhance the efficiency of the photocatalytic process. SA beads were doped with TiO₂ with or without different nanomaterials such as ZnO, SiO₂, and carbon nanotubes (CNTs). Mixing of TiO₂ with these nanomaterials was achieved to extend the wavelength range to the visible wavelength region. Methyl orange (MO) was used as an example of organic pollutants in the photocatalytic process using the batch photo-reactor. The photocatalytic process was executed by using ultraviolet or sunlight beams. The characterizations of the different types of prepared beads were examined using Fourier-transform infrared spectroscopy, X-ray diffraction, scanning electron microscopy, and thermogravimetric analysis. Also, the effect of different parameters on the photocatalytic efficiency of the prepared nanomaterials was studied. The results showed that SA beads doped with TiO₂ were able to degrade 97.9% under ultraviolet light, while in case of using SA beads doped with mixture of TiO₂ and SiO₂ were able to degrade 73.5% under sunlight after 5 h.

Keywords: Sodium alginate; Nanomaterials; Photocatalysis process; Water treatment

1. Introduction

Environmental pollution has far reaching negative consequences in the lives of humans. Degradation of organic pollutants, which have a deleterious effect on the well-being of mankind, has become a significant topic of research. The textile industry consumes considerable amounts of water during the dyeing and finishing operations [1]. The commonly used water treatment processes of industrial effluents, include chemical precipitation, lime coagulation, ion exchange, reverse osmosis, solvent extraction, and oxidation processes [2].

Chemical oxidation treatments are usually effective toward the destruction of chromophoric structures of dyes.

There are types of oxidation processes based on ozone, H₂O₂ and advanced oxidation process with photocatalysis. Problems with using ozone include its instability and its hazardous nature due to strong and non-selective oxidizing power. In this way the water coloration is removed, but often a complete mineralization is not achieved, chlorination, and ozonation cause decolorization by means of chemical reactions. The by-products of chlorination are chlorinated organics that may be more toxic than the dye itself. Heterogeneous photocatalysis is considered the most important technique in advanced oxidation processes (AOPs), which can be successfully used to oxidize many organic pollutants present in aqueous systems [3].

* Corresponding author.

The key advantage of the photocatalytic process is its inherent destructive nature, it does not involve mass transfer, it can be carried out under ambient conditions (atmospheric oxygen is sufficient as oxidant) and may lead to complete mineralization of organic carbon into CO_2 [4].

Photocatalytic degradation involves the use of certain semiconductors as catalysts for the production of the radicals. The use of titanium dioxide (TiO_2) as a catalyst for the photo-oxidation of organic compounds has received much interest because TiO_2 is plentiful, inexpensive, powerful, and environmentally friendly [3].

The process of semiconductor photocatalysis involves the following stages as shown in Fig. 1.

Light energy of a certain wavelength is made to fall onto a semiconductor. If the energy of the incident light is equivalent to the band gap energy of the semiconductor, electrons would be excited from the valence band to the conduction band of the semiconductor and holes would be left in the valence band. These electrons and holes could undergo subsequent oxidation and reduction reactions with any species, which might be adsorbed on the surface of the semiconductor to give the necessary products [5].

Sodium alginate (SA) is a polysaccharide extracted from brown algae, polymerize through 1,4-glycosidic bond from b-D-mannuronic acid (M unit) and a-L-guluronic acid (G unit). It is a non-toxic and naturally biodegradable green material which used as carrier for nanomaterials. The presence of sodium alginate as a biopolymer increases adhesion of nanoparticles. The use of alginate as a carrier material for nano-particles has enlightened the possibility of having a selective adsorption of organic molecules, depending on their electrical charge, due to interaction with the negative carboxylate groups on alginate [6,7].

Many efforts have been made to achieve the utilization of visible light for TiO_2 material, such as transitional metal ion (ZnO , SiO_2), non-metal element doping such as carbon nanotube (CNT). Nonmetal element doping narrows the band gap of TiO_2 by supplying a new hybrid energy band whose energy level is a little higher than that of the valence band of TiO_2 [8].

The aim of the present work is the treatment of the organic pollutant by preparation of sodium alginate beads doped with TiO_2 and different types of nanomaterials. The

performance of prepared polymeric beads in water treatment of organic pollutant using photocatalysis process was evaluated.

2. Experimental

2.1. Materials and chemicals

Sodium alginate (SA) was used as a polymeric substrate; it was supplied from BDH laboratory supplies, England. Glutaraldehyde (solution 50%) was used as a crosslinker, it was purchased from El Nasar Pharmaceutical Chemical Co. (ADWIC), Cairo, Egypt. Different nanomaterials that were used: titanium dioxide (TiO_2), P-25 anatase nano-powder, <25 nm particle size, zinc oxide (ZnO): nano-powder <100 nm particle size, silica (SiO_2): silica nano-particles, mesoporous, 200 nm particle size, pore size, carbon nanotube (CNT): O-D (10–15 nm), I-D (2–6 nm), assay >90% were supplied from Sigma Aldrich, Germany. Methyl orange that used as an example of organic matter was purchased from May & Baker Ltd., Dagenham, England. Other chemicals such as solvents and inorganic salts were of analytical reagent grade and used without further purification.

2.2. Apparatus and methods

2.2.1. Preparation of beads

Sodium alginate (SA) was dissolved by stirring in deionized water. The nano-particles (TiO_2 , ZnO , SiO_2 , and CNT) were dispersed in water through sonication for 1 h; this dispersion was mixed with the polymer solution. After mixing and forming of doped polymer solution with nanomaterials, the solution was poured as a drop-wise to form beads on a conical flask which containing crosslinking solution that contained glutaraldehyde in 75 acetone:25 water mixture. The obtained beads were left to harden in this solution for 24 h and then subsequently rinsed with tap water many times until pH reached to 7, then it was washed and stored in distilled water until used or characterized.

2.2.2. Photocatalytic experiments

Batch photoreactor consists of double jackets that were made of Pyrex. The inner tube has inside diameter of 5 and 35 cm long. The outer tube has the inside diameter of 10 and 30 cm long, as shown in Fig. 2.

A UV-C lamp with 15 W from low pressure mercury type lamp was installed in the center of the reactor, the outer tube was wrapped with protecting black foils for collecting all radiations of UV lamp inside the target component of methyl orange solution, air was purged in the solution using an air pump to make a good dispersion and a continuous motion of the used beads during the experiment. The experimental procedure was started after 30 min contact time in dark between the prepared methyl orange solution and the used beads that were charged into the reactor and obtaining a good distribution. After that, the UV lamp was turned on to initiate the photocatalytic process.

The sampling of the tested solution was made using a 10 mL volume syringe every 30 min. The concentration

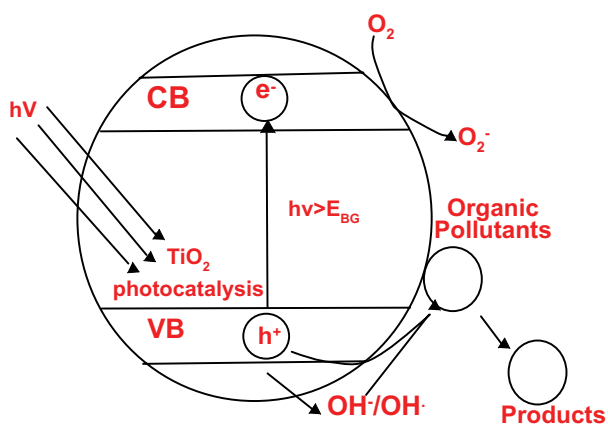


Fig. 1. Photocatalytic process.

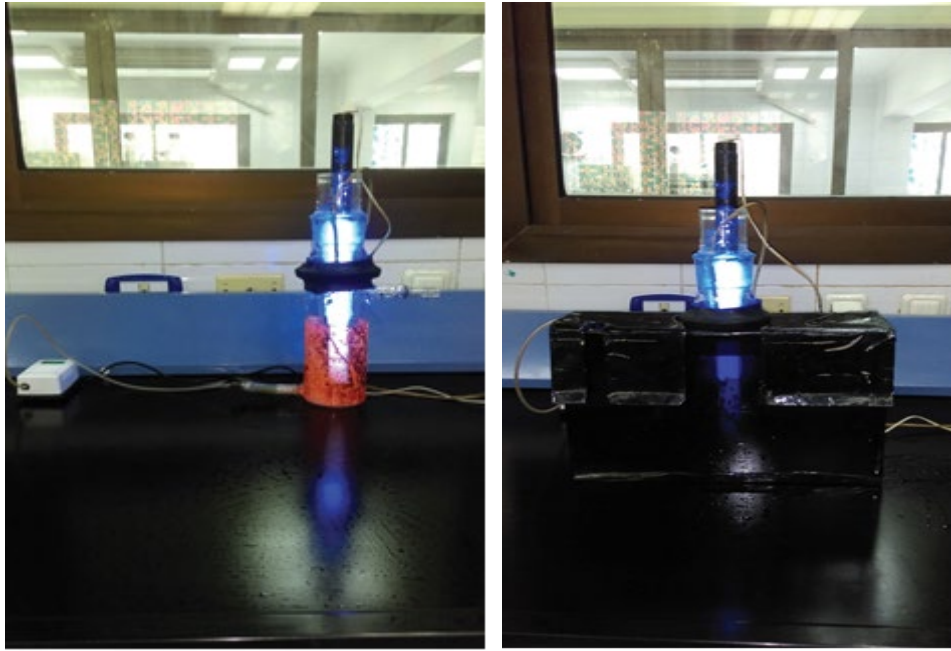


Fig. 2. Batch photoreactor.

change of methyl orange (MO) was determined by the UV-Vis spectrophotometer. The degradation rate of MO solution was calculated by the following formula:

$$D = \frac{C_0 - C}{C_0} \times 100\% = \frac{A_0 - A}{A_0} \times 100\% \quad (1)$$

where D is degradation rate, C_0 , A_0 and C , A are the concentration and absorbance of the MO solution at the absorption peak, 464 NM in adsorption equilibrium before and after UV irradiation, respectively.

2.3. Characterization of polymeric beads

2.3.1. Swelling, conversion, and gelation (%) measurements

The swelling, conversion, and gelation (%) for beads were measured as an indication of insoluble SA % in water. Dry beads of known weights were immersed in distilled water at 25°C until equilibrium has been reached. The beads were removed, plotted by absorbent paper and quickly weighed. The swelling percent was calculated as follows:

$$\text{Swelling}(\%) = \frac{(W_{\text{wet}} - W_{\text{dry}})}{W_{\text{dry}}} \times 100 \quad (2)$$

where W_{dry} and W_{wet} represent the weights of the dry and wet beads, respectively.

The percentage of both conversion and gelation of the prepared beads were calculated as follows:

$$\text{Conversion}(\%) = \frac{W_{\text{dry}}}{W_0} \times 100 \quad (3)$$

$$\text{Gelation}(\%) = \frac{W_{\text{dry hot}}}{W_0} \times 100 \quad (4)$$

where W_0 is the dry weight of the synthesized beads, W_{dry} and $W_{\text{dry hot}}$ are the dry weight of the resultant beads after impregnation in water at room temperature and at 50°C, respectively. W_{wet} is the weight of wet beads.

2.3.2. Fourier-transform infrared spectroscopy spectroscopy

Analysis by infra-red spectrophotometer was carried out by using Broker Vertex 70 Fourier-transform infrared spectroscopy (FTIR) spectrometer model.

2.3.3. X-ray diffraction

The crystalline structures of the prepared beads were analyzed by X-ray diffractometry (XRD) (X'Pert PRO, PANalytical, Netherlands) using Cu $K\alpha$ radiation in the angular region of $2\theta = 4^\circ - 70^\circ$. The instrument was operated at 40 KV and the spectra were recorded at scanning speed of 8°min^{-1} .

2.3.4. Thermo-gravimetric analysis

The thermal-gravimetric analysis (TGA) was carried out by using thermo-gravimetric analyzer TGA-50H atmosphere from nitrogen with a flow rate 20 mL/min and temperature rate holder $10^\circ \text{C}/\text{min}$. TGA of the samples was performed up to a temperature of 600°C , with a starting point at room temperature.

2.3.5. Scanning electron microscopy

The microscopic imaging of the neat and the doped SA beads with different nanomaterials was conducted using

scanning electron microscopy (SEM) FEI, Quanta 250 FEG (Netherlands) type.

2.3.6. UV/visible spectrophotometer

To determine the suitable wave length for measuring the absorption of the MO decoloration indication to degradation of total organic matter was using Unicam, model 300, England.

3. Results and discussion

3.1. Synthesis of sodium alginate beads

The optimum conditions of synthesis and crosslinking of SA were investigated through studying the effect of different parameters on swelling, conversion, and gelation (%). Such parameters included the polymer concentration, crosslinker type, and its concentration as well as the impregnation time in the crosslinker solution.

3.1.1. Effect of sodium alginate concentration

The effect of SA concentration on the swelling, conversion, and gelation (%) was studied using three different concentrations (3, 4, and 5 wt.%) of sodium alginate, as shown in Table 1.

From Table 1, the swelling % increased with the SA concentration due to the increase of functional groups of

OH to form the hydrogen bonds with the water molecules. On the other hand and in general, it gave acceptable values of both conversion and gelation %. These results agree well with that of the previous work of [9]. The polymer concentration, that was selected as best concentration for forming beads, was 4 wt.%.

3.1.2. Effect of crosslinker type

In the present study, different types of cross-linkers such as CaCl_2 , BaCl_2 , phosphoric acid, and glutaraldehyde were tested. The glutaraldehyde was selected as the best cross-linker. It gave polymeric beads with best mechanical stability. The model structure of prepared cross-linked SA by glutaraldehyde showed that there are two hydroxyl group (OH) of sodium alginate (SA) polymer react with the aldehyde group (CHO) of GA to form cross-links between the sodium alginate chains [10,12], as shown in Fig. 3.

3.1.3. Effect of crosslinker concentration

Different concentrations of glutaraldehyde ranged from 1.5 to 3 vol.% were used to investigate the optimum glutaraldehyde concentration, as shown in Table 2. As is obvious, the increase in cross-linker concentration lead to an increase in the conversion and the gelation % with decreasing of swelling %, because it decreases the number of the free functional groups of SA. The glutaraldehyde with 2 vol.% was selected as the optimum concentration due to it gave the highest swelling % with good conversion and gelation %.

3.1.4. Effect of impregnation time during the crosslinking process

Different impregnation times were tested to investigate the best time for the crosslinking of SA beads. The best time was 18 h, due to the high conversion and gelation % with good swelling %, as shown in Table 3.

Table 1

Effect of concentration of sodium alginate

SA concentration (wt.%)	Swelling (%)	Conversion (%)	Gelation (%)
3	58.8	93.3	88.7
4	67.1	95.1	90.9
5	75.6	92.9	91.5

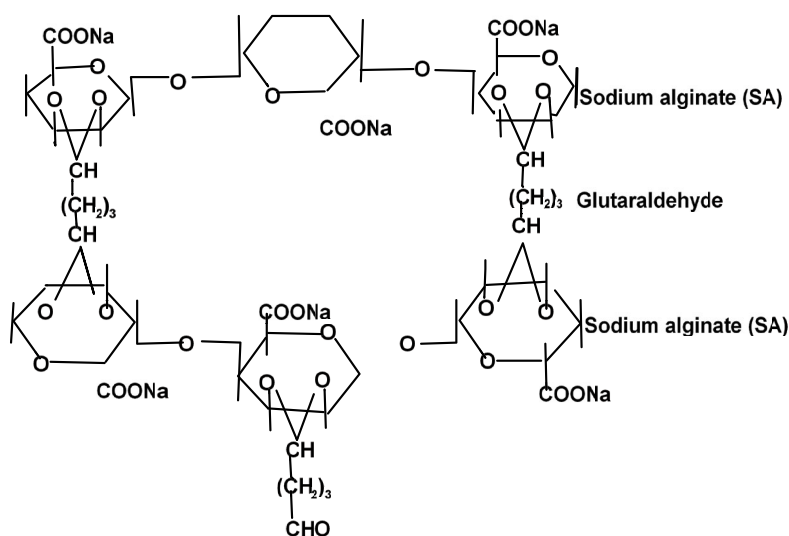


Fig. 3. Model structure of cross-linked SA with glutaraldehyde.

Table 2
Effect of cross-linker concentration

Cross-linker concentration (vol.%)	Swelling (%)	Conversion (%)	Gelation (%)
1.5	70.7	94.4	90.1
2.0	67.1	95.1	90.9
2.5	65.6	96.3	93.0
3.0	60.9	97.7	95.2

Table 3
Effect of impregnation time in the cross-linker

Impregnation time (h)	Swelling (%)	Conversion (%)	Gelation (%)
12	70.3	93.8	89.1
18	67.1	95.1	90.9
24	64.1	95.1	90.9

3.2. Synthesis of SA/TiO₂ nanocomposite beads

Modification of SA beads by TiO₂ nanoparticles was carried out to use the modified beads in water treatment via photodegradation process. The effect of TiO₂ concentration onto swelling, conversion, and gelation % was studied, as shown in Table 4.

It is evident from Table 4 that the increase of TiO₂ concentration lead to a decrease of swelling % and a decrease of both conversion and gelation %. TiO₂ with concentration of 4 wt.% was selected. In the subsequent experiments as it gave moderate conversion and gelation % with an acceptable swelling %.

3.3. Synthesis of SA doped with mixture of TiO₂ and different nanomaterials

Modification of SA beads by mixing of TiO₂ with different nanomaterials was achieved. The effect of nanomaterial type included ZnO, SiO₂, CNT, and its concentration related to TiO₂ onto swelling, conversion, and gelation % was studied as shown in Tables 5–7, respectively.

The obtained results showed that the increase in both ZnO and SiO₂ nanoparticles content lead to increase the swelling % and the vice versa with CNT. This due to the nature of metal oxide nanoparticles of both ZnO and SiO₂ that may form hydrogen bonds between the oxygen atoms of nanoparticles with hydrogen atom of water. On the other hand, the hydrophobicity of CNT leads to decrease the swelling % of prepared beads.

3.4. Characterization of the different polymeric beads

3.4.1. FTIR spectroscopy

The FTIR spectra of neat SA beads and modified with different concentration of TiO₂ with or without different nanomaterials were evaluated as shown in Fig. 4.

Table 4
Effect of concentration of TiO₂ nanoparticles

Concentration of TiO ₂ nanoparticles/SA (W/W)	Swelling (%)	Conversion (%)	Gelation (%)
0.005	76.3	94.0	93.0
0.01	73.4	93.6	92.9
0.02	70.5	93.3	91.9
0.04	65.0	93.0	91.7
0.08	61.8	91.0	90.5

Table 5
Effect of concentration of TiO₂ with ZnO nanoparticles

Ratio (TiO ₂ :ZnO) nanoparticles (0.04 wt.%)	Swelling (%)	Conversion (%)	Gelation (%)
(100:0)	65.0	93.0	91.7
(75:25)	85.8	97.2	95.5
(50:50)	89.9	95.8	94.2
(25:75)	97.9	97.1	93.1
(0:100)	111.0	96.7	95.9

Table 6
Effect of concentration of TiO₂ with SiO₂ nanoparticles

Ratio (TiO ₂ :SiO ₂) nanoparticles (0.04 wt.%)	Swelling (%)	Conversion (%)	Gelation (%)
(100:0)	65.0	93.0	91.7
(75:25)	89.4	96.2	93.2
(50:50)	92.0	96.5	91.5
(25:75)	111.6	95.6	92.0
(0:100)	131.1	96.4	97.1

Table 7
Effect of concentration of TiO₂ with SiO₂ nanoparticles

Ratio (TiO ₂ :CNT) nanoparticles (0.04 wt.%)	Swelling (%)	Conversion (%)	Gelation (%)
(100:0)	65.0	93.0	91.7
(75:25)	70.6	91.0	88.6
(50:50)	68.6	93.1	90.5
(25:75)	66.7	95.8	91.6
(0:100)	60.4	91.2	87.8

The obtained results were in agreement with the previous work [10]. It was found that two main characteristic peaks were observed for neat SA beads at 1,729 and 3,367 cm⁻¹ which corresponded to C=O and O–H groups, respectively, Fig. 4a. On the other hand, the FTIR spectra of modified SA beads modified with TiO₂ shown in Fig. 4b. It is obvious that there is TiO₂ characterized band at 704.47 cm⁻¹ and other stretching vibration of Ti–O–Ti peak at 1,409 cm⁻¹, these results were in agreement with

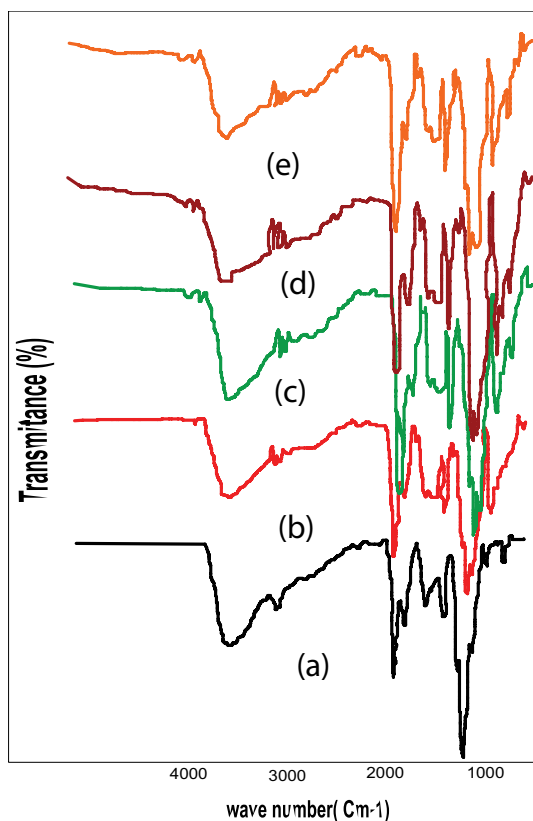


Fig. 4. FTIR spectra for (a) cross-linked alginate, (b) (SA/TiO₂), (c) (SA/TiO₂ + SiO₂), (d) (SA/TiO₂ + ZnO), and (e) (SA/TiO₂ + C).

the previous work [11]. While, for SA beads doped with mixture of TiO₂ and different nanomaterial, as shown in Figs. 4c–e. There were strong peaks appearing at 1,128.44 and 759.48 cm⁻¹ corresponding with Si–O–Si bond, Fig. 4c. While with ZnO metal oxide, Fig. 4d, a peak appeared at 609.22 cm⁻¹. In case of CNT, Fig. 4e, there is no significant peak was observed. These results were in agreement with previous works [12–14].

3.4.2. XRD patterns

SA is usually semi-crystalline due to strong interaction between the alginate chains through intermolecular hydrogen bonding [15]. Fig. 5a shows four peaks for the sodium alginate cross-linked beads that can be seen at $2\theta = 14^\circ, 23^\circ, 25^\circ,$ and 44° indicating SA crystallinity. On the other hand, The XRD pattern of modified SA beads modified with TiO₂ are shown in Figs. 5b–d. It is obvious that the increasing the number of peaks with increasing the amount of TiO₂ in composites and the intensity of TiO₂ characteristic peaks for anatase which are used at $2\theta = 25.4^\circ, 48^\circ$ increases with increasing amount of TiO₂ loaded on sodium alginate polymer (SA). The smallest peaks of the XRD graph reveal the crystalline size [11]. The peaks corresponding the anatase TiO₂ phase appeared at $2\theta = 25.3^\circ, 37.8^\circ, 48.0^\circ, 54.4^\circ,$ and 62.8° [5]. While, for SA beads doped with mixture of TiO₂ and different nano-material, as shown in Figs. 5e–g. There were peaks appearing at $2\theta = 25^\circ$, Fig. 5e [12]. While with ZnO metal oxide, Fig. 5f, the small peak appeared at $2\theta = 37^\circ$ [16]. In case of CNT, Fig. 5g, there were peaks at $2\theta = 26^\circ$ [17].

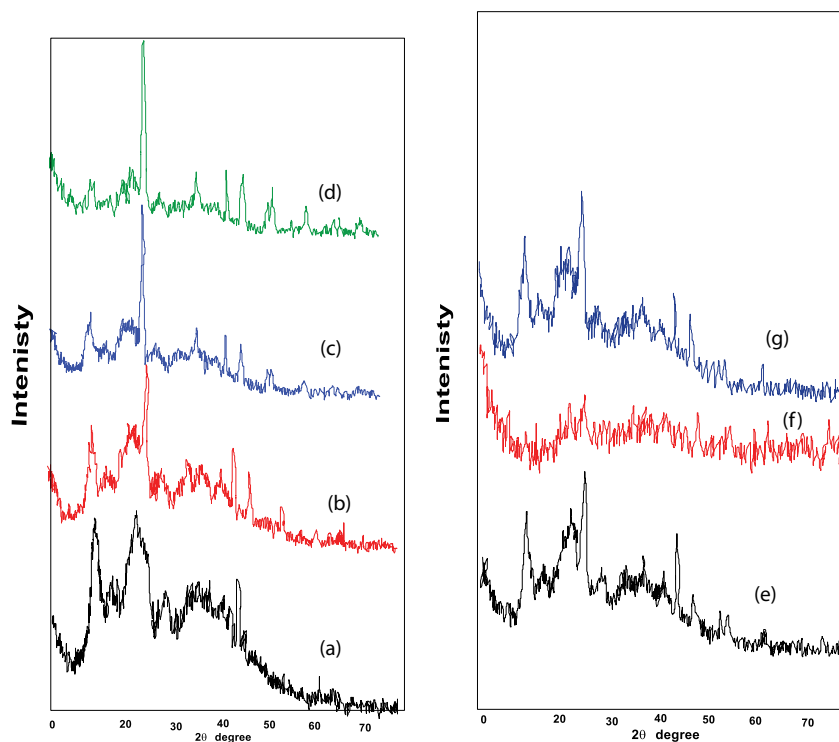


Fig. 5. XRD for (a) cross-linked alginate, (b) (SA/TiO₂)_{0.02}, (c) (SA/TiO₂)_{0.04}, (d) (SA/TiO₂)_{0.08}, (e) (SA/TiO₂ + SiO₂), (f) (SA/TiO₂ + ZnO), and (g) (SA/TiO₂ + C).

3.4.3. SEM analysis

All SA beads images with SEM were exhibited a relatively regular spherical shape. The outer surface was rather rough and corrugated with many folds and creases, which would increase contact surface area between organic dyes and the composite beads, and provide more active sites, thus improving their adsorption performances, as shown in Fig. 6a, and this result was in agreement with previous work of [18]. By doping SA with TiO_2 , (Figs. 6b–d) reveal the dispersion of TiO_2 nanomaterial from low to high concentrations. By increasing TiO_2 concentration, there was an agglomerated of nanomaterial on the surface. Images of beads in Figs. 6e–g reveal the SA doped with mixture of TiO_2 and different nanomaterials, there rough appearance caused by the presence nanomaterial, which organize themselves as aggregates throughout the NaAlg matrix [19].

3.4.4. TGA analysis

Studying of the influence of heating rate in the thermal behavior sodium alginate was performed under both air and N_2 atmospheres. Since every synthetic or natural polymer containing hydrophilic groups usually presents strong interaction with water, the humidity content may effectiveness their properties and is an important characteristic to be determined [20]. The thermal stability of SA

beads, as shown in Fig. 7, showed that the initial weight loss of the polymer may have been caused by the presence of moisture in the sample (40°C – 100°C). In the second region, the percent weight loss was caused by the loss of CO_2 from the polysaccharide backbone of the polymer. As there were COO^- groups in the sodium alginate, it would decarboxylate in this temperature range (230°C – 280°C). In the temperature range between 460°C and 560°C , the weight loss might have been caused by the loss of abundant hydroxyl groups on the polysaccharide in the form of water. Sodium alginate was not completely degraded in this temperature range. It maintained a weight percent of about 30% at 500°C . A residue of about 3% was retained up to 600°C . These results were in agreement well with previous work [21].

The thermal stability sodium alginate doped with TiO_2 nano-particles is presented in Fig. 7b. It is obvious that it gave more or less the same thermal degradation behaviour of sodium alginate as shown in Fig. 7a but with a different residue weight loss that reached to 23% at 600°C . This may be due to the interaction and formation of the hydrogen bonds or other coordinate bonds between the TiO_2 nanoparticles and polymeric chains [22,23].

The thermal stability of SA beads that modified with mixture of TiO_2 and different nano-materials as shown in Figs. 7c–e. Fig. 7c shows that the thermal stability of SA/ $\text{TiO}_2 + \text{SiO}_2$ gives 9% weight loss. On the other hand, the thermal stability of SA/ $\text{TiO}_2 + \text{ZnO}$, as is clear in Fig. 7d,

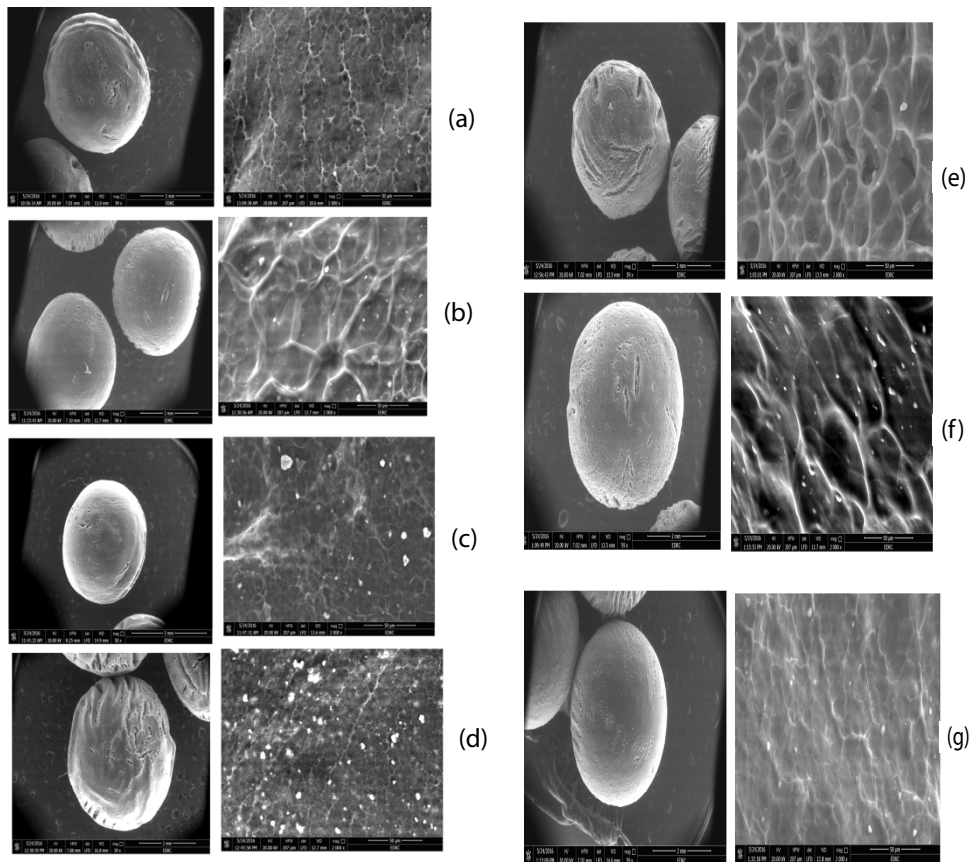


Fig. 6. SEM for (a) cross-linked alginate, (b) $(\text{SA}/\text{TiO}_2)_{0.02}$, (c) $(\text{SA}/\text{TiO}_2)_{0.04}$, (d) $(\text{SA}/\text{TiO}_2)_{0.08}$, (e) $(\text{SA}/\text{TiO}_2 + \text{SiO}_2)$, (f) $(\text{SA}/\text{TiO}_2 + \text{ZnO})$, and (g) $(\text{SA}/\text{TiO}_2 + \text{C})$.

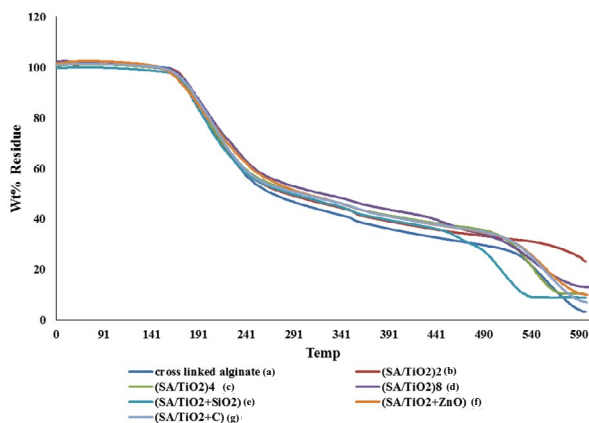


Fig. 7. TGA for (a) cross-linked alginate, (b) $(SA/TiO_2)_{0.02}$, (c) $(SA/TiO_2 + SiO_2)$, (d) $(SA/TiO_2 + ZnO)$, and (e) $(SA/TiO_2 + C)$.

shows the same thermal degradation of sodium alginate with a weight loss of 10% at 600°C. The thermal stability of SA/TiO_2 + CNTs presented in Fig. 7e shows the same thermal degradation of sodium alginate with 7% weight loss at 600°C. Oxidation temperatures for CNTs vary from material-to-material, but are quite typical in the range of 400°C–650°C [24].

3.5. Photocatalytic activity

Methyl orange is one of the most important classes of commercial dyes, it has very short excited-state lifetime, it is stable to visible and near UV light and provide a useful probe for photoredox reactions [25], the molecular structure of MO is shown in Fig. 8.

The degradation of MO was studied to evaluate the performance of different nanocomposite beads types of SA/TiO_2 with or without different metal oxide nano-materials such as; ZnO , SiO_2 , and CNT. The Photocatalysis experiments were carried out under both UV and solar radiation. All the experiments were done at room temperature ($27^\circ C \pm 2^\circ C$). The operation conditions included pH range 3–12, dye concentrations ranged from 10 up to 50 mg/L using different concentrations of nanomaterials.

The optimum wavelength for measuring the absorbance of methyl orange decolorization with time at pH = 3.5 equal 506 nm, but for pH = 7 and 10 the optimum wavelength is 464 nm. The photodegradation efficiency was observed by measuring the absorbance of the solution samples at its maximum absorption wavelength of 464 nm with UV-Vis spectroscopy, as shown in Fig. 9.

The decolorization efficiency as a function of time was calculated by the absorbance of the original and analytical samples. Seven milliliters of sample were performed at interval time from 30 min up to 5 h.

3.5.1. Factors affecting on using of sodium alginate doped with TiO_2 under UV Light

3.5.1.1. Effect of time on the degradation of MO dye

Time of the photodegradation may be one of the necessary factors in the photocatalytic process. The photodegradation of various illumination times using $SA/(TiO_2)_{0.04}$

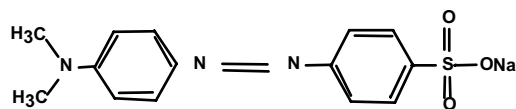


Fig. 8. Molecular structure of methyl orange.

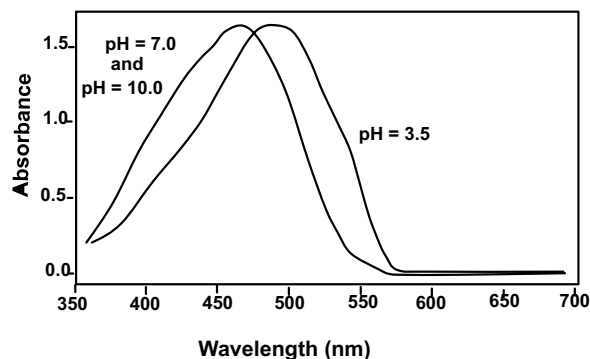


Fig. 9. Absorption spectra of MO 20 ppm in aqueous solution.

nanocomposite beads. The dye concentration was equal 20 mg/L, and initial pH value equal 5, as shown in Fig. 10. It is clear that 240 min illumination time is the optimum time for the photocatalytic degradation.

3.5.1.2. Effect of TiO_2 nanoparticles concentration

Fig. 11 shows the photodegradation results using sodium alginate beads doped with TiO_2 different concentrations. The operation conditions included dye concentration equal 20 mg/L, reaction time equal 5 h, pH value equal 5. It was believed that as the amount of catalyst increased, the number of photons absorbed and the number of dye molecules absorbed were increased owing to an increase in the number of catalyst particles. But actually above a certain level of catalyst loading, a screening effect of excess particles occurred and all the catalyst surfaces could not be exposed to illumination. That is, the increase of catalyst loading beyond a certain limit could not effectively increase the photocatalytic reaction rate [25].

3.5.1.3. Effect of initial dye concentration

The effect of initial dye concentration ranged from 2.5 to 50 mg/L on the rate of decolorization efficiency of MO using $SA/(TiO_2)_{0.04}$ nanocomposite beads at pH = 5, presented in Fig. 12. The results showed that as the initial concentration of methyl orange increased the reaction rates decreased which most probably due to the increased concentration affects light penetration into the methyl orange solution. Similar behaviors were reported previously [25].

3.5.1.4. Effect of pH values

The effect of pH was studied by keeping all other experimental conditions constant and changing the initial pH value between 3 and 10. The degradation efficiency was studied with $SA/(TiO_2)_{0.04}$ using initial dye concentration of 20 ppm. The results are illustrated in Fig. 13. A decrease in

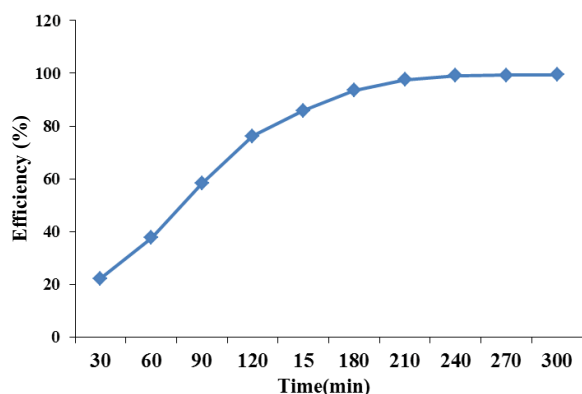


Fig. 10. Effect of time on the degradation of MO dye; 4 wt.% SA/TiO₂, 20 ppm MO concentration, pH 5.

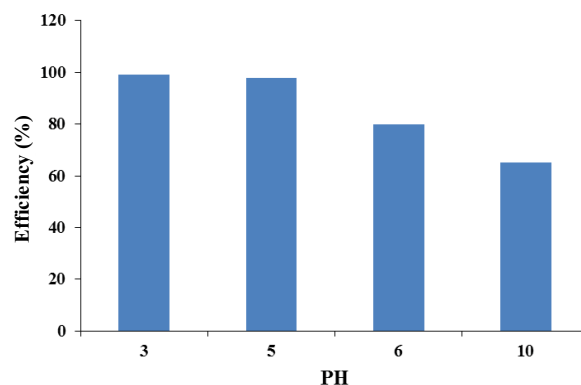


Fig. 13. Effect of pH on the photo-degradation efficiency of (SA/TiO₂)_{0.04} at constant time.

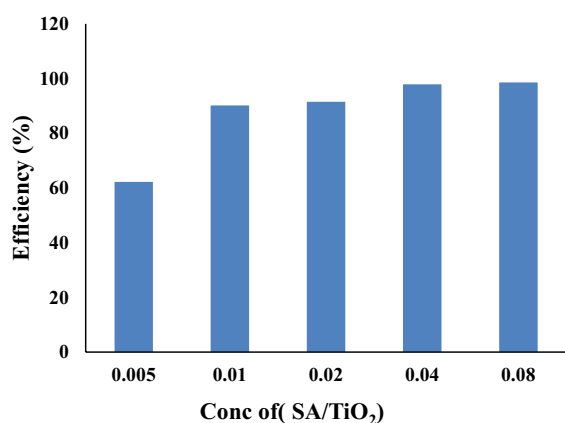


Fig. 11. Effect of TiO₂ nanoparticles different concentration on the photo-degradation efficiency at constant time.

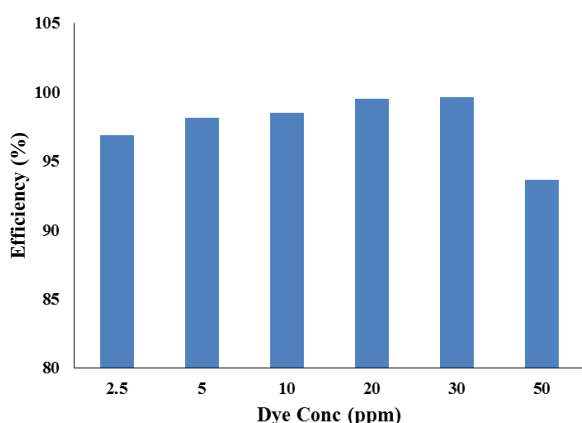


Fig. 12. Effect of initial MO dye concentration on the photo-degradation efficiency.

decolorization rate can be seen with increasing pH up to 10. Higher pH retarded the formation of OH[•] radicals and decreased the photocatalytic reaction rate [9]. At low pH, reduction by electrons in conduction band may play an important role in the degradation of azo dye [25].

3.5.2. Effect of photodegradation on using of sodium alginate doped with TiO₂ and another metal oxide (ZnO, SiO₂) or non-metal (CNT) under UV light

The results are illustrated in Fig. 14. The performance of photodegradation was increased in case of doping TiO₂ with ZnO under UV light. However, the band edges of these semiconductors lie in the UV region which makes them inactive under visible light irradiation. TiO₂ which has a band gap of 3.2 eV is superior to other semiconductor oxides due to its high chemical stability, low cost and nontoxic nature. ZnO which has a similar band gap of about 3.2 eV is sometimes preferred over TiO₂ for degradation of organic pollutants due to its high quantum efficiency [8].

3.5.3. Effect of photodegradation on using of sodium alginate doped with TiO₂ and another metal oxide (ZnO, SiO₂) or non-metal (CNT) under sun light

The results are illustrated in Fig. 15. The performance of photodegradation were increased in case of doping TiO₂ with SiO₂ under sun light, this is due to the lower band gap of silicon, maximize the range of wavelength in the visible light regionals shown in Fig. 16.

The addition of SiO₂ effectively suppresses the particle size and TiO₂ phase transformation from anatase to rutile, Ultraviolet light covers only 5% of solar energy so that the addition of TiO₂ is a majority of solar energy that could alternatively be used to promote the reaction [26].

The degradation efficiency under visible light irradiation by using TiO₂/SiO₂ was much better than that of TiO₂ or SiO₂ alone. This may be to the high surface area and great adsorption of TiO₂/SiO₂ particles facilitated electron injection so as to significant increased the rate of photodegradation of methyl orange. Moreover, the TiO₂/SiO₂ particles had good sedimentation ability and high thermal stability [5].

In the case of doped TiO₂ with CNT, the degradation up to 39% due to fusing CNT with TiO₂ at the nanoscale level promotes the separation of those electron-hole charges generated upon, CNTs could exhibit either metallic or semi-conducting behavior (band gap can vary from zero to ~2 eV) by tuning diameter and helicity, CNTs have two kinds of crucial roles when enhancing the photocatalytic activities of TiO₂. One is to act as an electron reservoir, which helps

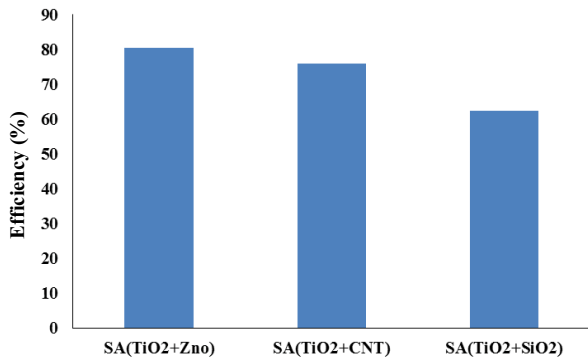


Fig. 14. Effect of photodegradation on using sodium alginate doped with TiO₂ and another metal oxide (ZnO, SiO₂) or non-metal (CNT) under UV light.

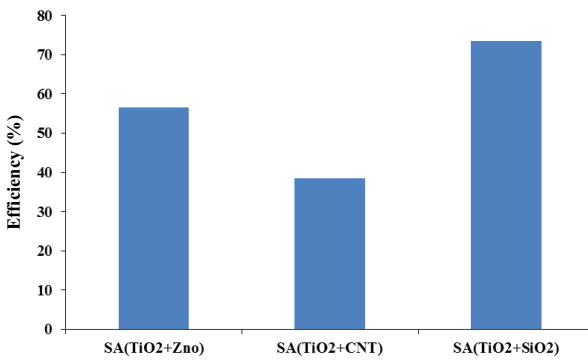


Fig. 15. Effect of photodegradation on using of sodium alginate doped with TiO₂ and another metal oxide (ZnO, SiO₂) or non-metal (CNT) under sunlight.

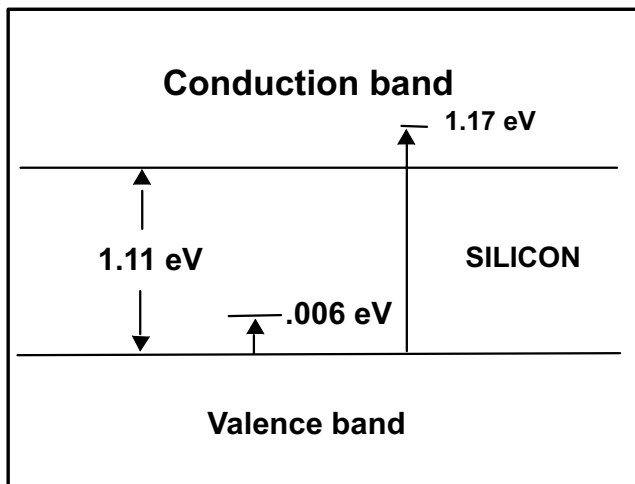


Fig. 16. Bandgap of silicon.

to trap electrons emitted from TiO₂ particles due to irradiation by UV-light, therefore hindering electron-hole pair's recombinations. The other is to act as a dispersing template or support for controlling the morphology of TiO₂ particles within the TiO₂-CNT nanocomposites [27].

3.5.4. Kinetic study

The kinetics of UV-degradation of MO at concentration of 20 ppm under UV-irradiation is illustrated in Fig. 17. The results show that the photocatalytic decolorization of MO dye can be described by the first order kinetic model, $\ln(C_0/C) = kt$, where C_0 is the initial concentration and C is the concentration at time t . The plots of the concentration data gave a straight line. The rate constant was found to be 0.0096 min⁻¹ with a correlation factor 0.9663. The photocatalytic degradation kinetic indicated that the destruction rate of photocatalytic oxidation of MO dye over illuminated TiO₂ fitted the Langmuir-Hinshelwood (L-H) kinetics model [28,29].

3.5.5. Reusability of SA/(TiO₂)_{0.04} nanocomposite beads

Recovery and reuse is another advantage for SA/TiO₂ photocatalytic degradation nanocomposite beads, which is very important in practical applications. The reproducibility of the photocatalytic degradation activity was performed with a constant MO concentration (20 mg/L) and 10% beads catalyst dose (SA/TiO₂)_{0.04} for each cycle. The regeneration of the catalyst was done by the following a simple way. After the photocatalytic degradation of the MO solution process, the beads were draw and washed with distilled water. The recovered SA/TiO₂ nanocomposite bead was reused in the next cycle Fig. 18. It was found that the

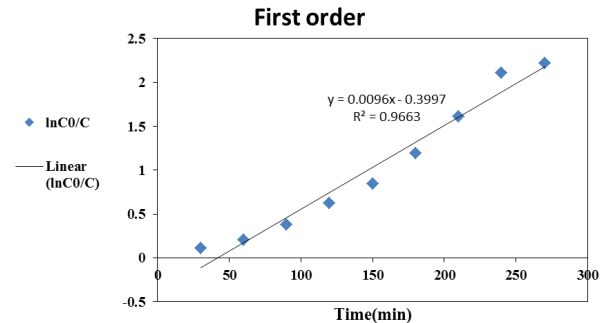


Fig. 17. Pseudo-first-order kinetics for MO photocatalyzed degradation.

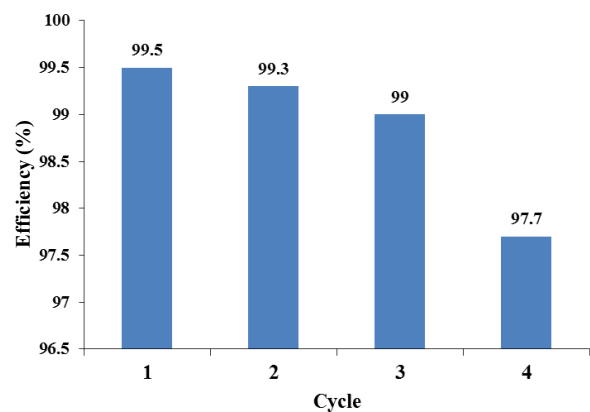


Fig. 18. Reuse of (SA/TiO₂)_{0.04} nanocomposite beads.

degradation efficiency of methyl orange was more than 95% for four cycles.

4. Conclusions

A novel crosslinked SA nanocomposite with high swelling capacity and relatively high adsorption efficiency for methyl orange dye was prepared. The methyl orange solution was successfully decolorized by the photocatalytic reaction under weak illumination conditions. It was also found that pH is another important parameter in determining the reaction rate and the acidic condition was favorable for the methyl orange and using of TiO₂ only is favourable under UV radiation. The higher initial concentration decreased the light penetration thus decreased the relative reaction rate of photocatalytic reaction. It was obvious that there was an optimum amount of catalyst loading which does not prevent screening effect to illumination. The photocatalytic oxidation of methyl orange dye has been studied using (1) sodium alginate polymer doped with TiO₂, (2) Sodium alginate doped with TiO₂ and another nanomaterials. The obtained results showed that sodium alginate hydrogel beads doped with TiO₂ only was able to degrade 97.9% of methyl orange solution after 5 h under ultra-violet light, while that with TiO₂ and SiO₂ was able to degrade 73.5% of methyl orange solution under sun light. The photo-oxidation of dye followed pseudo-first-order kinetics, which fitted the Langmuir–Hinshelwood model. Therefore, the nanocomposite is hopeful to be used in degradation of organic pollutants. Further investigation is in progress.

Acknowledgment

It is a pleasure to acknowledge the financial support provided by the Science and Technological Development Fund (STDF) in Egypt through Grant 5240 (Egyptian Desalination Research Center of Excellence, EDRC).

References

- [1] D. Chatterjee, S. Dasgupta, Visible light induced photocatalytic degradation of organic pollutants, *J. Photochem. Photobiol., C*, 6 (2005) 186–205.
- [2] N. Ahalya, T.V. Ramachandra, R.D. Kanamadi, Biosorption of heavy metals, *Res. J. Chem. Environ.*, 7 (2003) 71–79.
- [3] E. Bizani, K. Fytianos, I. Poullos, V. Tziridis, Photocatalytic decolorization and degradation of dye solutions and wastewaters in the presence of titanium dioxide, *J. Hazard. Mater.*, 136 (2006) 85–94.
- [4] A.R. Khataee, M.B. Kasiri, Photocatalytic degradation of organic dyes in the presence of nanostructured titanium dioxide: influence of the chemical structure of dyes, *J. Mol. Catal. A: Chem.*, 328 (2010) 8–26.
- [5] Y. Chen, K. Wang, L. Lou, Photodegradation of dye pollutants on silica gel supported TiO₂ particles under visible light irradiation, *J. Photochem. Photobiol., A*, 163 (2004) 281–287.
- [6] M.H. Abdel Rehim, M.A. El-Samahy, A.A. Badawy, M.E. Mohram Packing, Photocatalytic activity and antimicrobial properties of paper sheets modified with TiO₂/sodium alginate nanocomposites, *Carbohydr. Polym.*, 148 (2016) 194–199.
- [7] Y. Hu, T. Chen, X. Dong, Z. Mei, Preparation and characterization of composite hydrogel beads based on sodium alginate, *Polym. Bull.*, 72 (2015) 2857–2869.
- [8] S. Rehman, R. Ullah, A.M. Butt, N.D. Gohar, Strategies of making TiO₂ and ZnO visible light active, *J. Hazard. Mater.*, 170 (2009) 560–569.
- [9] M.M. Abo El-Fadl, A.M. El-Aassar, A.A. Mohamed, Synthesis of nanocomposite membranes and their application in photocatalytic process for organic pollution removal from groundwater, East Nile Delta, Egypt, *Desal. Water Treat.*, 55 (2015) 2951–2961.
- [10] B.V.K. Naidu, K.V.S.K. Rao, T.M. Aminabhavi, Pervaporation separation of water + 1,4-dioxane and water + tetrahydrofuran mixtures using sodium alginate and its blend membranes with hydroxyethylcellulose—a comparative study, *J. Membr. Sci.*, 260 (2005) 131–141.
- [11] V. Vetrivel, K. Rajendran, V. Kalaiselvi, Synthesis and characterization of pure titanium dioxide nanoparticles by sol-gel method, *Int. J. ChemTech Res.*, 7 (2015) 1090–1097.
- [12] P.A. Sajid, T. Devasena, Synthesis and characterization of silica nanocomposite for bone application, *Int. Res. J. Pharm.*, 3 (2012) 173–177.
- [13] G. Xiong, U. Pal, J.G. Serrano, K.B. Ucer, R.T. Williams, Photoluminescence and FTIR study of ZnO nanoparticles: the impurity and defect perspective, *Phys. Status Solidi C*, 3 (2006) 3577–3581.
- [14] J.H. Lehman, M. Terrones, E. Mansfield, K.E. Hurst, V. Meunier, Evaluating the characteristics of multiwall carbon nanotubes, *Carbon*, 49 (2011) 2581–2602.
- [15] S. Thakur, S. Pandey, O. Arotiba, Development of a sodium alginate-based organic/inorganic superabsorbent composite hydrogel for adsorption of Methylene blue, *Carbohydr. Polym.*, 153 (2016) 34–46.
- [16] Y. Lu, J. Zhang, L. Ge, C. Han, P. Qiu, S. Fang, Synthesis of novel AuPd nanoparticles decorated one-dimensional ZnO nanorod arrays with enhanced photoelectrochemical water splitting activity, *J. Colloid Interface Sci.*, 483 (2016) 146–153.
- [17] X. Chun Song, Y.F. Zheng, Y. Zhao, H.Y. Yin, Hydrothermal synthesis and characterization of CNT@MoS₂ nanotubes, *Mater. Lett.*, 60 (2006) 2346–2348.
- [18] X. Li, H. Lu, Y. Zhang, F. He, L. Jing, X. He, Fabrication of magnetic alginate beads with uniform dispersion of CoFe₂O₄ by the polydopamine surface functionalization for organic pollutants removal, *Appl. Surf. Sci.*, 389 (2016) 567–577.
- [19] F. Karkeh-Abadi, S. Saber-Samandari, S. Saber-Samandari, The impact of functionalized CNT in the network of sodium alginate-based nanocomposite beads on the removal of Co(II) ions from aqueous solutions, *J. Hazard. Mater.*, 315 (2016) 224–233.
- [20] J.P. Soares, J.E. Santos, G.O. Chierice, E.T.G. Cavalheiro, Thermal behavior of alginic acid and its sodium salt, *Eclat. Quim.*, 29 (2004), ISSN 1678–4618.
- [21] T. Tripathy, R.P. Singh, Characterization of polyacrylamide-grafted sodium alginate: a novel polymeric flocculant, *J. Appl. Polym. Sci.*, 81 (2001) 3296–3308.
- [22] J.F. Li, X. Zhen-Liang, Y. Hu, Y. Li-Yun, L. Min, Effect of TiO₂ nanoparticles on the surface morphology and performance of microporous PES membrane, *Appl. Surf. Sci.*, 255 (2009) 4725–4732.
- [23] Yang, Y., Wang, P., Zheng, Q. Preparation and properties of polysulfone/TiO₂ composite ultrafiltration membranes, *J. Polym. Sci., Part B: Polym. Phys.*, 44 (2006) 879–887.
- [24] N. Gull, S.M. Khan, M.A. Munawar, M. Shafi, F. Anjum, M.T. Zahid Butt, T. Jamil, Synthesis and characterization of zinc oxide (ZnO) filled glass fiber reinforced polyester composites, *Mater. Des.*, 67 (2015) 313–317.
- [25] W. Nam, J. Kim, G. Han, Photocatalytic oxidation of methyl orange in a three-phase fluidized bed reactor, *Chemosphere*, 47 (2002) 1019–1024.
- [26] C.S. Kim, J.W. Shin, S.H. An, H.D. Jang, T.O. Kim, Photodegradation of volatile organic compounds using zirconium-doped TiO₂/SiO₂ visible light photocatalysis, *Chem. Eng. J.*, 204–206 (2012) 40–47.
- [27] M. Božič, V. Vivod, R. Vogrinčič, I. Ban, G. Jakša, S. Hribernik, D. Fakin, V. Kokol, Enhanced catalytic activity of the surface

- modified TiO₂-MWCNT nanocomposites under visible light, *J. Colloid Interface Sci.*, 465 (2016) 93–105.
- [28] J. Cunningham, G. Al-Sayyed, S. Srijaranai, Chapter 22: Adsorption of Model Pollutants onto TiO₂ Particles in Relation to Photo-Remediation of Contaminated Water, G. Helz, R. Zepp, D. Crosby, Eds., *Aquatic and Surface Photochemistry*, Lewis Publications, CRC Press, Boca Raton, FL, 1994, pp. 317–348.
- [29] A. Olivira-Campose, O. Peter, L. Poullos, Photocatalytic Degradation Studies on Malachite Green, In: *Environment 2010: Situation and Perspectives for the European Union* 6–10 May 2003, Porto, Portugal, 2003, pp. 1–6.